GEOPHYSICS, VOL. 71, NO. 4 (JULY-AUGUST 2006); P. SI139–SI150, 25 FIGS.
10.1190/1.2216190

The virtual source method: Theory and case study

Andrey Bakulin[1] and Rodney Calvert[1]

ABSTRACT

We present a way to image through complex overburden. The method uses surface shots with downhole receivers placed below the most complex part of the troublesome overburden. No knowledge of the velocity model between shots and receivers is required. The method uses time-reversal logic to create a new downward-continued data set with virtual sources (VS's) at the geophone locations. Time reversal focuses energy that passes through the overburden into useful primary energy for the VS. In contrast to physical acoustics, our time reversal is done on a computer, utilizing conventional acquisition with surface shots and downhole geophones.

With this approach, we can image below extremely complex (realistic) overburden — in fact, the more complex the better. We recast the data to those with sources where we actually know and can control the waveform that has a downward-radiation pattern that may also be controlled, and is reproducible for 4D even if the near-surface changes or the shooting geometry is altered slightly.

To illustrate the method, we apply the VS technique to a synthetic, elastic example with extreme heterogeneity, where conventional approaches fail to image the data. A 4D field-data example shows that the VS method (VSM) enables sensitive reservoir monitoring below a complex, time-variant near surface that is not achievable with surface 4D seismic or conventional 4D vertical seismic profiling (VSP).

INTRODUCTION

Overburden complexity represents a major obstacle for seismic imaging. Large and rapid velocity variations in all spatial directions lead to strong scattering that severely distorts and disperses wavefronts propagating both downward to the reflectors and returning upward. In these circumstances, conventional imaging techniques based on geometrical ray theory or other approximations might not adequately describe the wave propagation and thus might produce poor results. Wave-equation imaging could give better results, provided that a detailed velocity model of the overburden has been constructed. Obtaining an accurate velocity model, however, remains a problem for all imaging approaches.

In conventional seismic surveys, both sources and receivers are located at the earth's surface. Because of its downhole recording, VSP leads to higher-frequency images (Hardage, 2000). It is commonly believed that these higher-frequency VSP images are the result of the fact that signal crosses the near surface only once, and a measured wavelet is available for better deconvolution. Nevertheless, conventional VSP imaging are still requires a velocity model to be constructed for the near surface in order to perform imaging of the deeper subsurface.

In crosswell and single-well seismology, both sources and receivers are placed in the boreholes, further increasing frequency content and completely avoiding near-surface and overburden distortions. This, however, requires use of downhole sources as well as receivers.

The goal of this paper is to present a new method that sits in between the VSP and crosswell and single-well seismic. Although we utilize original, VSP-type acquisition with downhole sensors and surface shots, we generate data corresponding to downhole source-receiver configurations. Our time-reversal technique, combined with downhole recording, allows us to undo all transmission effects of the near surface and thus completely eliminate overburden velocity model building from the imaging process. The resulting wavefield corresponds to a new configuration, with both downhole sources and receivers sitting under the overburden. As downhole sources are simulated on a computer at the locations of borehole geophones, they are called *virtual sources*; thus we name this approach the virtual source method (VSM). The VSs have several advantages over real sources. We can control their wavelet and, to some extent, the radiation pattern. These sources also have some attractive properties, such as radiating downward only and exciting longitudinal waves with no associated shear, or shear with no associated longitudinal.

The VSM is built on three general principles: time reversibility, reciprocity, and linearity. We start with a review of the physics be-

Manuscript received by the Editor March 14, 2005; revised manuscript received August 19, 2005; published online August 17, 2006.
[1]Shell International Exploration and Production, 3737 Bellaire Boulevard, Houston, Texas 77025. E-mail: andrey.bakulin@shell.com; rodney.calvert@shell.com.

hind our approach and then describe a simple algorithm for generation of VS data. We apply the method to a synthetic data set with an extremely complex near surface and compare its imaging capabilities with those of conventional approaches. Then we review additional advantages offered by the VSM for 4D seismic monitoring. Finally, we present a field-data example with 4D VSP in which the VSM does an excellent job of imaging and sensitive monitoring below a complex and changing near surface.

TIME-REVERSAL CONSIDERATIONS

To illustrate the physical principles involved in the new approach, let us consider the simple experiment depicted on Figure 1a. The source emits the signal, and waves propagate in all directions through a heterogeneous medium. Then a receiver array records the wavefield at each point of a closed surface surrounding the source. The received wave motion can be reproduced in reverse time if each of the receivers is converted into a source and emits the recorded wavefield in time-reversed chronology (Figure 1b). This property arises from the fact that wave equation contains only a second derivative with respect to time, and thus displacement fields $\mathbf{u}(\mathbf{x},t)$ and $\mathbf{u}(\mathbf{x},-t)$ are both solutions of the same equation. In our simple experiment, the time-reversed signal gives rise to waves that travel toward the center and collapse exactly at the receiver placed in the location of the original source (Figure 1b). Such a proposition is attractive because (Fink et al., 2000; Fink and Prada, 2001)

- The observation surface can be adequately sampled by a finite number of receivers distributed with spacing no larger than half the smallest wavelength.
- In practice, recording can be performed over a limited angular/spatial area only;
- there is no restriction on medium complexity because time reversal holds for any type of media that could be acoustic, elastic, arbitrarily heterogeneous, and anisotropic (but not absorptive or nonlinear).

Many numerical and laboratory experiments with ultrasound have confirmed these findings robustly (Chakroun et al., 1995; Draeger et al., 1998; Fink et al., 2000; Fink and Prada, 2001; Tsogka and Papanicolaou, 2002; Blomgren et al., 2002). It also has been noticed that after the energy collapses back into the original-source position, the waves start to radiate again away from the original source (de Rosny and Fink, 2002). To explain this, recall that in the forward experiment, the source brought external energy into the system that excited waves. Therefore, to faithfully replay this scenario back in time, energy brought by collapsed waves should be taken out of the system at the (original) source location. Then we would observe complete rest, consistent with the original state before the source.

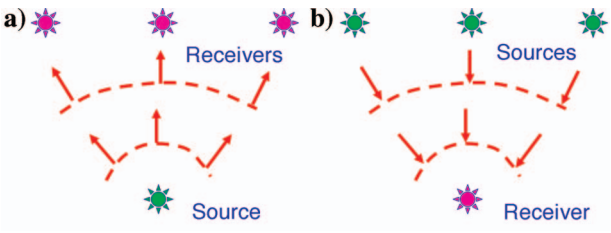

Figure 1. Simple experiment with forward (a) and reverse (b) wave propagation explaining time reversal.

In our approach, these converging waves power the VS that fires in the subsurface at the very moment when energy collapses into its location. Time reversal ensures that, apart from edge effects, during collapse energy is focused at the VS point and is zero everywhere else. After release of this energy in the form of outgoing waves, we would observe normal forward wave propagation as if it had been induced by a real physical source placed at the VS location. Such an approach allows us to simulate a VS at any true receiver point inside the medium by sources that are far away. Because we directly measure the transmission responses between the surface sources and receivers at depth and therefore between the VS and each of the surface sources, we are able to focus energy back to the VS point by time reversal. Thus we do not require the knowledge of medium velocities between the sources and the receivers. Since time reversal is by nature a full wave-equation method, the VS approach does not place any restriction on complexity of the medium separating the VS from the actual source array. Moreover, in certain cases, complexity of this separating medium is beneficial in creating better VSs with wider radiation patterns than if the intervening medium is simple.

THE VIRTUAL SOURCE METHOD

In our VS approach, we propose acquisition geometry similar to VSP (Figure 2). The preferred configuration would be a strongly deviated well, possibly along a curved 3D trajectory, so that a significant part of the underlying deeper subsurface will be imaged. Such a well does not have to be deep because the requirement is to have geophones below the most complex overburden. We do not have to limit this overburden complexity.

To remove the damaging distortions (including multiples) of the near surface, we transform the original surface-to-downhole data to a new, completely downhole configuration with VSs placed at the receiver locations (Figure 2). Such a transformation follows the cartoon described in the previous section and requires three main steps:

1) Select the downhole geophone where a VS needs to be created (red triangles in Figure 2)
2) Record the wavefield from each surface shot to the selected VS geophone and time reverse it
3) Backpropagate (on a computer) the time-reversed wavefield from the whole source array to selected VS geophone and record the resultant summation at each of the downhole receivers

To achieve analogy with the cartoon from Figure 1, we must employ the reciprocity principle. Because in practice we use real sourc-

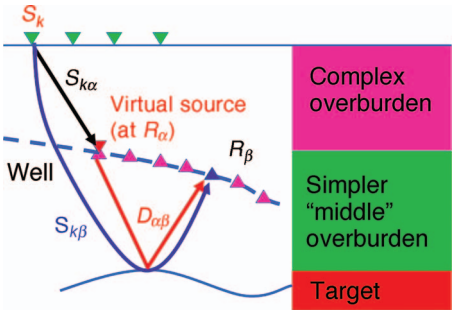

Figure 2. VS experiment: Receivers in the borehole record both the downgoing wavefield through the heterogeneous near surface (black arrow) and reflected signal from the deeper targets (red arrow).

es at the surface, reciprocity allows us to substitute input acquisition with surface sources and downhole receivers as a data set equivalent to the one acquired with surface sensors and downhole excitation. Unklike the cartoon in Figure 1, our reverse propagation is done on the computer in order to avoid repeated acquisition. We can do this because we want to focus the energy on the image rather than in physical space, which is required in some medical applications, such as acoustic kidney stone removal (Fink et al., 2000). In practice, an additional deconvolution step is required to ensure that various physical sources are equated to a common, desired VS excitation.

The result of the third step is a virtual shot gather corresponding to a fixed downhole VS and array of existing geophones (red trace in Figure 2). We can apply similar principles to obtain a VS at any subsurface point where we do not actually have a downhole geophone. This, however, will be possible only when an accurate velocity model of the surrounding media is known or can be derived. The placement of a geophone at the location of the VS removes that requirement, and time reversal provides an exact answer without any knowledge of the velocity model between the sources and the receivers. In the case of very heterogeneous overburden, such downhole recording may be preferred over any attempt to derive an accurate velocity model from the surface seismic alone.

SYNTHETIC CASE STUDY (IMAGING)

Let us examine the feasibility of the VS approach on a complex, synthetic data set resembling some features of the field case study described in the final section. At each step, we compare corresponding results obtained with the VSM and conventional approaches.

Model and acquisition geometry

In Figure 3, longitudinal- and shear-wave velocities are displayed. The deeper part of the model is represented by several layers with a target reservoir between 562 and 590 m deep. The main complexity arises from glacial, fluvial deposits occupying 240 m of the upper near surface. Because a good velocity model for the near surface was not available, we created a synthetic model with velocity rapidly varying in both lateral and vertical directions. P-wave velocity in the near surface varies between 900 m/s and 2900 m/s, and S-wave velocity varies between 350 m/s and 1200 m/s. No intrinsic attenuation is assumed in the model.

Acquisition geometry consisted of 80 vertical geophones with 10-m spacing sitting in a horizontal well at a depth of 430 m (Figure 3). A surface line of shots was simulated by 321 explosion sources buried at 15-m depth and spaced at 5 m. All shots have identical wavelet shape.

Synthetic input data

A representative gather recorded by a fixed, buried receiver is shown in Figure 4. The wavefield is extremely complex because of scattering happening in the near surface. To appreciate the distortions caused by the near surface, let us examine the wavefield between the first arrivals and the yellow line in Figure 4. For display purposes, we introduced hyperbolic moveout correction based on the moveout of the yellow line and show a window above that line in Figure 5. It is clear that applying only kinematic compensation in the form of static corrections cannot eliminate the distortions caused by the near surface. This distortion from a coherent wavefront is strong and is both spatially and dip-dependent. Figure 5 shows substantial phase and amplitude disruptions varying from shot to shot: The shapes and amplitudes of the wavelets differ, the number of peaks and troughs varies, and scattered diffractions and reverberations are present. If static corrections cannot recover the first arrivals, which represent the most robust part of the wavefield, then they will be unable to heal weaker reflections that suffer even more from overburden distortions.

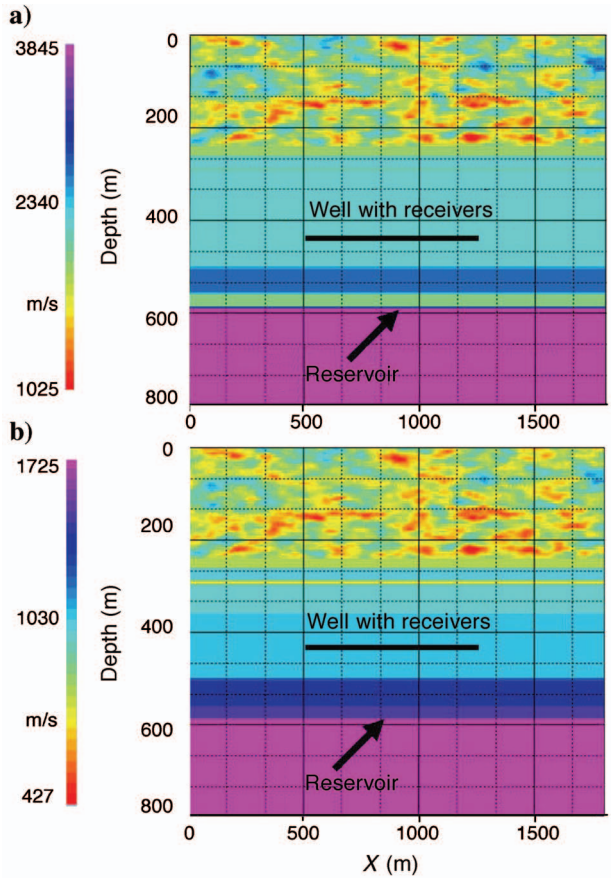

Figure 3. P-wave (a) and S-wave (b) velocity models used in the synthetic case study.

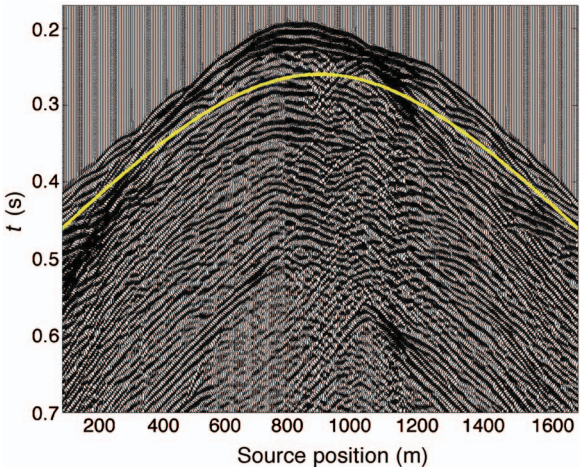

Figure 4. Raw receiver gather (X = 900 m). The response is for the vertical component of displacement from explosion sources.

Generation of VS data

A simplified version of VS data can be generated according to the following simple correlation algorithm. First, a location of a VS is selected at the position of any downhole receiver, say R_α (Figure 2). Then we select receiver R_β, where a corresponding output trace will be computed. For a zero-offset trace, $\alpha = \beta$, and the same receiver location is picked twice. Downhole seismic trace $D_{\alpha\beta}(t)$ for a selected VS-receiver pair is estimated by the simple formula

$$D_{\alpha\beta}(t) = \sum_{k=1}^{N} S_{k\alpha}(-t) * S_{k\beta}(t), \quad (1)$$

where $S_{k\beta}(t)$ is trace recorded from the kth source at the surface by receiver R_β; $S_{k\alpha}(-t)$ is the time-reversed portion of the trace recorded from source S_k by receiver R_α at the VS location; and * denotes convolution. Summation is carried either over the whole aperture of the surface-source array or over a limited portion around location α with a maximum number of source elements N. Note that equation 1 can also be formally written as a crosscorrelation of the original traces (without time reversing one of them); however, current convolution form is more closely tied to physically intuitive time-reversal interpretation.

Link to time reversal

Let us demonstrate that equation 1 describes the time-reversal process outlined above. The actual trace from source S_k to receiver R_β can be represented as

$$S_{k\beta}(t) = w_k(t) * \tilde{S}_{k\beta}(t), \quad (2)$$

where $\tilde{S}_{k\beta}(t)$ is the earth's impulse response, and $w_k(t)$ is the source waveform.

If the source wavelet $w_k(t)$ is replaced by the time-reversed trace $S_{k\alpha}(-t) = w_k(-t) * \tilde{S}_{k\alpha}(-t)$, then we obtain a new trace for the same source-receiver pair

$$N_{k\beta}(t) = S_{k\alpha}(-t) * \tilde{S}_{k\beta}(t) = w_k(-t) * \tilde{S}_{k\alpha}(-t) * \tilde{S}_{k\beta}(t), \quad (3)$$

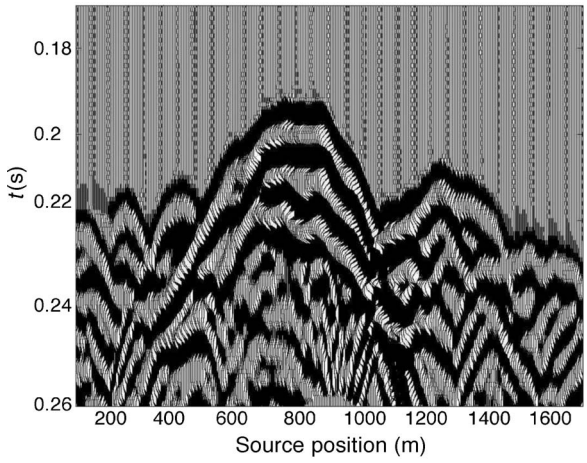

Figure 5. Zoom-in of first arrivals above yellow line on Figure 4. Hyperbolic moveout correction has converted yellow hyperbola into a horizontal line along the bottom axis of this figure.

that corresponds to the following single-channel, time-reversal experiment (Figure 6):

- A wavefield is emitted from source at R_α and recorded by receiver at S_k as shown on Figure 6a (due to reciprocity, such trace $S_{\alpha k}(t)$ is equivalent to the real measured trace $S_{k\alpha}(t)$ emitted from the source S_k and read by the receiver R_α).
- This trace is retransmitted back in time-reversed chronology from the source S_k and results in recording $N_{k\beta}$ at another receiver R_β (Figure 6b). This contrasts with Figure 2, which depicts the special case when the trace is read by the receiver R_α coinciding with the location of the original source.

True multichannel time reversal is a superposition of single-channel experiments described above with an additional constraint of a consistent wavelet for each experiment, i.e., $w_k(t) = w(t)$:

$$\hat{R}_{\alpha\beta}(t) = \sum_{k=1}^{N} N_{k\beta}(t) = w(-t) * \sum_{k=1}^{N} \tilde{S}_{k\alpha}(-t) * \tilde{S}_{k\beta}(t), \quad (4)$$

where summation is performed along the source array. This constraint is necessary to ensure that we time reverse the wavefield corresponding to the same excitation.

If we rewrite equation 1 in the new notations,

$$D_{\alpha\beta}(t) = w(t) * w(-t) * \sum_{k=1}^{N} \tilde{S}_{k\alpha}(-t) * \tilde{S}_{k\beta}(t), \quad (5)$$

and compare with equation 4, we recognize a time-reversal experiment with an autocorrelation wavelet, that is, an experiment with a wavelet that has been perfectly phase-deconvolved, but has the source amplitude spectrum squared. Therefore, equation 1 describes a time-reversal process under the assumption of the constant wavelet shape throughout the array.

Can time reversal be improved?

Time reversal and equation 1 should work in an ideal situation when a closed acquisition surface completely surrounds the VS location. In practice, the acquisition geometry is restricted, and surface shots have different coupling and signature. We believe that, in this case, time-reversal equation 1 can be improved and generalized as

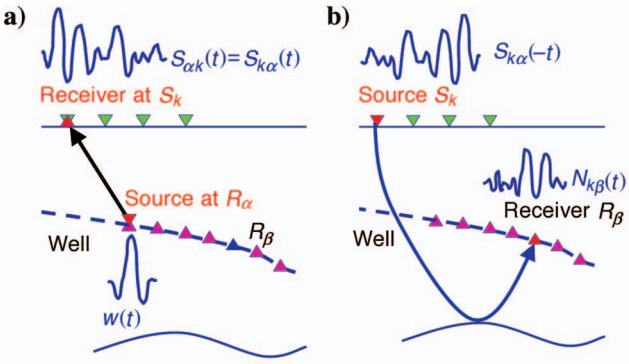

Figure 6. Forward wave propagation with wavelet $w(t)$ (a) and single-channel, time-reversal experiment (b) explaining equations 1–3.

$$D_{\alpha\beta}(t) = \sum_{k=1}^{N} S_{k\beta}(t) * M(t) * S_{k\alpha}^{-1}(t), \quad (6)$$

where $S_{k\alpha}^{-1}(t)$ is the inverse of the downgoing part of $S_{k\alpha}(t)$, and $M(t)$ is a chosen source wavelet within the available bandwidth.

A surface shot at S_k produces a downgoing signal $S_{k\alpha}(t)$ at R_α. Invoking linearity, if this source at k was additionally convolved with $M(t)*S_{k\alpha}^{-1}(t)$, where $S_{k\alpha}^{-1}(t)$ is the inverse $S_{k\alpha}(t)$, then we would receive a pulse $M(t)$ at downhole location R_α at time zero. When we do the same for all shots S_k, all of these results arrive in-phase at time zero. If the corrected, downgoing signals are carried forward into positive time, we have this energy radiating from a receiver at α with wavelet $M(t)$. This is the essence of our VS.

What is the difference between using the inverse $S_{k\alpha}^{-1}(t)$ and the time reverse $S_{k\alpha}(-t)$ to correct for overburden response between surface shot S_k and downhole point R_α? A real surface shot will have some unknown response with a ghost and coupling response. In travelling from S_k to R_α, there may be some attenuation and reverberation filtering. If we use $S_{k\alpha}(-t)$ as a correction filter, then all of these responses will be time-reversed and applied to the data again, resulting in data filtered by the autocorrelation of the ghost, coupling response, etc. Although the data will have correct phase, the amplitude spectral distortions will be squared. Applying $S_{k\alpha}^{-1}(t)$ corrects for the amplitude effects of the sources and overburden as well as the phase. In practice, a simple procedure is to first apply $S_{k\alpha}(-t)$ and then derive the amplitude correction that shapes the autocorrelation $S_{k\alpha}(t)*S_{k\alpha}^{-1}(t)$ to a desired pulse $M(t)$. This is the route we followed for the field case study below, while on the synthetic example, we used the simplified time-reversal approach described by equation 1.

What if we acquired our data by shooting on a surface that completely surrounded R_α, made no upward and downward wave separations, there were no transmission losses, and all the source wavelets were identical? The time-reversal filter $S_{k\alpha}(-t)$ would also correct for the multiples and reverberations from the physical shots entering R_α, but not those caused by the radiation pattern from R_α, both up and down. It may be more practical and advantageous to restrict our acquisition to a surface patch and generate a downward-radiating VS and apply simple dereverberation and source-amplitude correction to $S_{k\alpha}(-t)$.

VS gathers

The resulting VS gather is depicted on Figure 7a. The central trace corresponds to zero offset or coinciding VS and receiver. This can be compared with the surface-to-downhole records of Figure 4. We now begin seeing coherent hyperbolic events: one with $t_0 \approx 80$ ms is the first interface below VS, while another at $t_0 \approx 140$ ms is the bottom reservoir. To illustrate that VS data indeed correspond to a downhole configuration, let us compare the gather obtained with a separately computed data set wherein we fire physical sources at the downhole locations instead of VSs. Wavelet shape for downhole sources is the same as for surface sources. Such a comparison (depicted on Figure 7b) shows that VS data closely resemble the true downhole data set with all useful PP reflections clearly visible. The match is not precise for two reasons: first, the VS data set has a zero-phase autocorrelation wavelet different from signal in the synthetic downhole data set; second, we muted later parts of the time-reversed traces and thus eliminated certain unwanted reflections, as described in Appendix A.

Figure 8 shows a similar comparison between VS and directly simulated downhole data for two other VS locations along the borehole profile. The match between the two is surprisingly good up to the longest offset recorded. Appendix B shows that reconstruction of long offsets on VS records results from extreme scattering in the near surface and that it would be impossible to achieve in the presence of a homogeneous overburden. Therefore, we see that the VSM generates a downhole data set without knowledge of the overburden velocity model and that a complex overburden can actually help.

In these demonstrations, we have used a 2D model. In a real application we would like to use an areal configuration of surface shots to generate a VS with a 3D radiation pattern. Even with a 2D line of sources above a 3D heterogeneous overburden, however, our VS honors the 3D overburden, but it will have a restricted crossline radiation pattern unless the overburden is extremely heterogeneous.

Comparing images with surface and VS data

Let us compare images obtained with VS data with conventional surface-to-downhole data. To obtain an image with conventional surface-to-downhole data, a full overburden velocity model, including the near surface, needs to be constructed. With the quality of the raw data illustrated in Figure 4, we were unable to perform velocity model building from the data themselves.

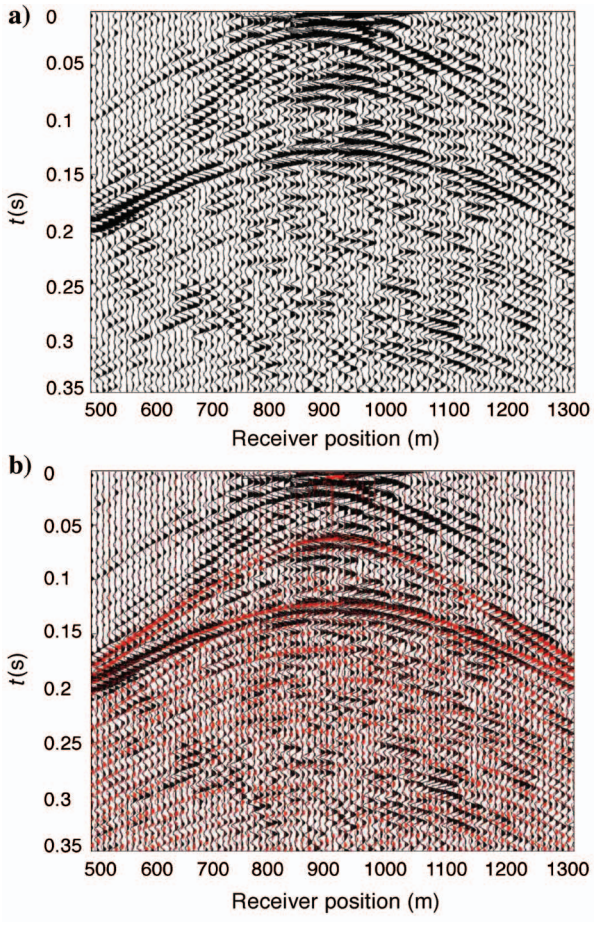

Figure 7. (a) VS gather computed for VS at $X = 900$ m. (b) Same VS gather (black), but overlaid by a downhole gather (red) computed for a physical, downhole source (explosion) placed at the location of the VS. A good match is observed between PP reflections on both records.

Therefore, we performed the comparison with the exact velocity model used for generating the original surface-to-downhole data. Although we will never know the exact model in real life, this would represent a best possible scenario, showing a limit of conventional imaging techniques.

Kirchhoff prestack depth migration (PSDM) of the original surface-to-downhole data produces a good quality section (Figure 9b) that correctly images plane interfaces, including the bottom reservoir at 590 m. The level of noise is also quite reasonable, taking into account that the imaging relied on ray theory only. Figure 9a shows the corresponding depth image of the VS data. The two images are of similar quality, but they differ in one substantial point: the VS image was obtained without any knowledge of the near-surface velocity model between sources and receivers, while the conventional image required the exact velocity model of the entire overburden. To obtain the VS image, we needed only the lower 1D portion of the velocity model below 430 m, which is easily obtainable from the prestack VS data.

Finally, VS introduces an additional advantage over the real downhole sources in suppressing unwanted radiation toward the surface that generates reflections from above. As explained in Appendix C, this is because of the downward-oriented radiation patterns of the VSs.

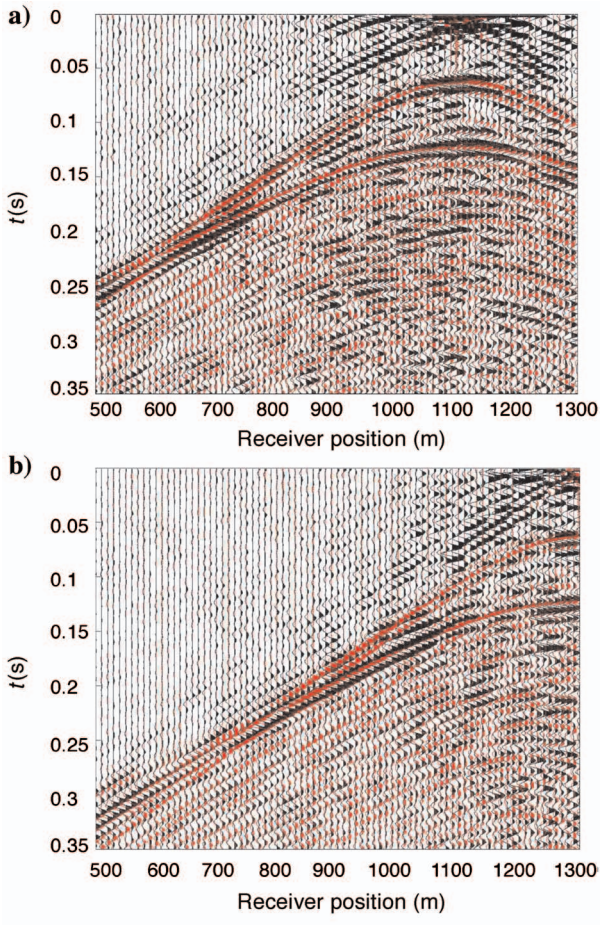

Figure 8. Same comparison as in Figure 7b, but for VS at X = 1100 m (a) and X = 1300 m (b).

SYNTHETIC CASE STUDY — 4D MONITORING

The fact that a velocity model above the receivers is not required for creating VS data has far-reaching implications for 4D seismic monitoring that aims to identify the locations of changes in the reservoir and to quantify those changes in terms of fluid movement or pressure variation. To obtain truly reservoir-caused 4D changes in practice, we need to overcome two significant challenges, namely measurement changes and near-surface changes:

1) If we are unable to repeat exactly the positions of the shots and receivers, then in each survey, waves travel through different parts of the overburden and thus produce different seismic traces even in the absence of subsurface changes. These differences will mask or reduce the ability to detect real 4D reservoir changes.
2) Changes in the near surface such as tides, water table movement, and freezing/thawing may cascade down the seismic response and generate artificial 4D differences at a reservoir level.

The VS approach substantially reduces the negative impact of both nonrepeatable acquisition and changing overburden. In the remainder of this synthetic study, we show how VS can correct for nonrepeatable shot locations. We illustrate the second point directly on real data in the following section.

For simplicity, assume that we have illuminated the same earth model with two different acquisition lines shifted with respect to each other by only 5 m in the inline direction. This results in a large difference field that starts with the first arrivals (Figure 10). This difference can be partly reduced by introducing 4D static corrections on the order of 2–3 ms. The remaining difference is still large and displays a false 4D response over the whole record.

The nonrepeatability between two corresponding traces a and b from each survey is often quantified by the so-called normalized root-mean-square (rms) difference:

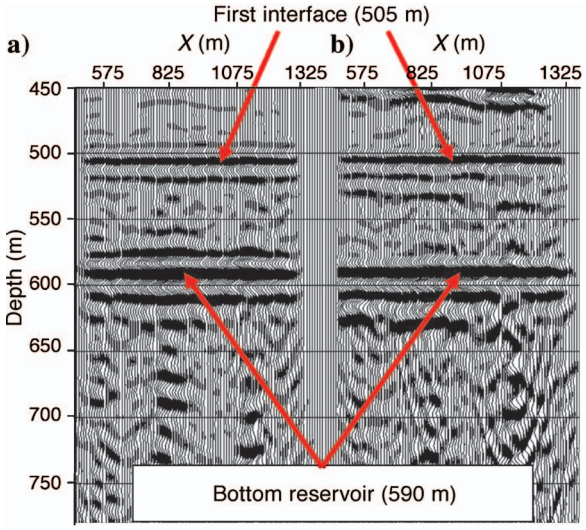

Figure 9. PSDM images obtained with VS data (a) and original surface-to-downhole data (b). The VS image (a) needs a velocity model only below 430 m where the receivers are, whereas the conventional image (b) required an exact velocity model of the entire overburden, including the near surface.

$$\text{Nrms} = \frac{\text{rms}(a-b)}{\text{rms}(a)+\text{rms}(b)} \times 200\%, \tag{7}$$

$$\text{rms}(a) = \sqrt{\frac{\sum_{i=L}^{M} a^2(t_i)}{M-L}}, \tag{8}$$

where $t_L \le t \le t_M$ is the selected time interval. The Nrms averaged over the receiver gather before static corrections can be as high as 140%. That is similar to the Nrms for a pair of random traces (Figure 11a). Notice that traces with larger offsets are less repeatable than those with smaller offsets, probably because of a longer travel path through the near surface. Introduction of static corrections reduces the Nrms (Figure 11b) but still leaves it above 50%. Subtle 4D signal from reservoirs may easily be lost in such a noisy unrepeatable background. Therefore, even a 5-m shift in shot positions can render 4D monitoring useless for a heterogeneous near surface.

A similar experiment with VS data shows that they withstand the nonrepeatable shot acquisition much better. Using two different shot lines, we generated two separate VS data sets (Figure 12a). Despite different shot locations within the surface-source array, no static corrections are necessary to match the two VS data sets. Indeed, the VSs remained stationary, because the geophones are at fixed locations in the borehole, and time reversal has made corrections automatically. The difference between the two VS gathers (Figure 12b) is substantially smaller at all times and offsets, as supported by the Nrms computations (Figure 13). To preserve similar aperture in angle terms, the largest offset used for migration was about 800 m for surface and 200 m for the VS data. Comparing Nrms curves for corresponding maximum offsets from Figure 11b and Figure 13, we find that the VS data have an Nrms two to three times smaller than that of the surface data: the VS data are much less sensitive to exact configuration of the surface source array. We conclude that the VSM can relax the requirement to repeat the exact source locations, thus mitigating one important problem for 4D monitoring.

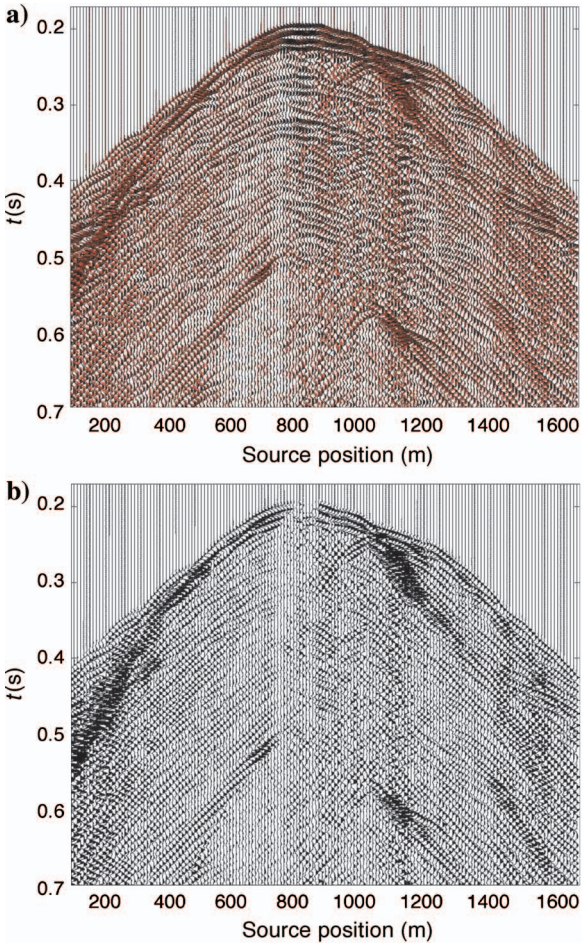

Figure 10. (a) Surface-to-downhole receiver gather from first (black) and second (red) shot lines for a fixed receiver at $X = 900$ m. (b) Difference between two receiver gathers above shown with the same amplification.

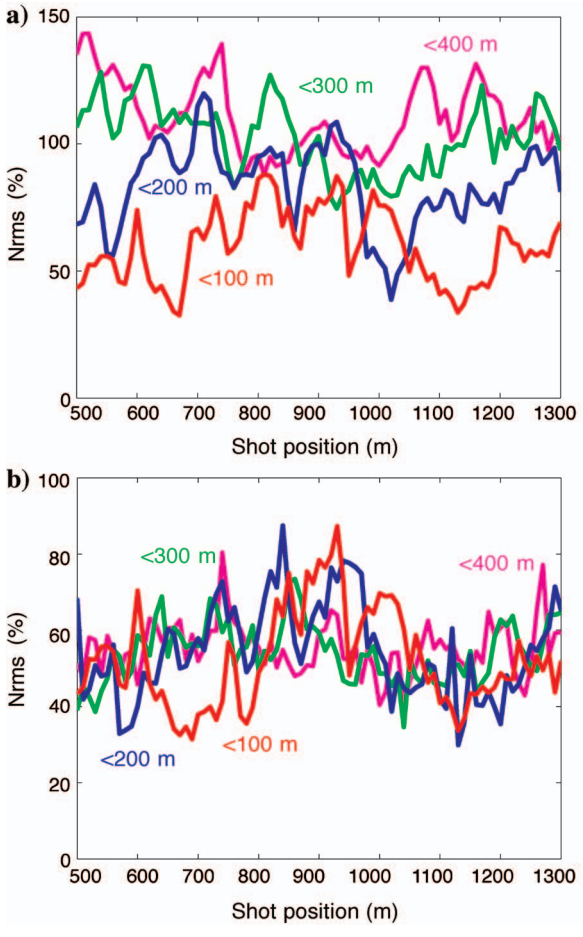

Figure 11. (a) Averaged Nrms over the whole shot gather for raw surface-to-downhole data shown as a function of shot position. The number for each plot identifies the maximum offset used in each shot gather. A time window $0 \le t \le 700$ ms is used. (b) Same as (a) but with static corrections introduced.

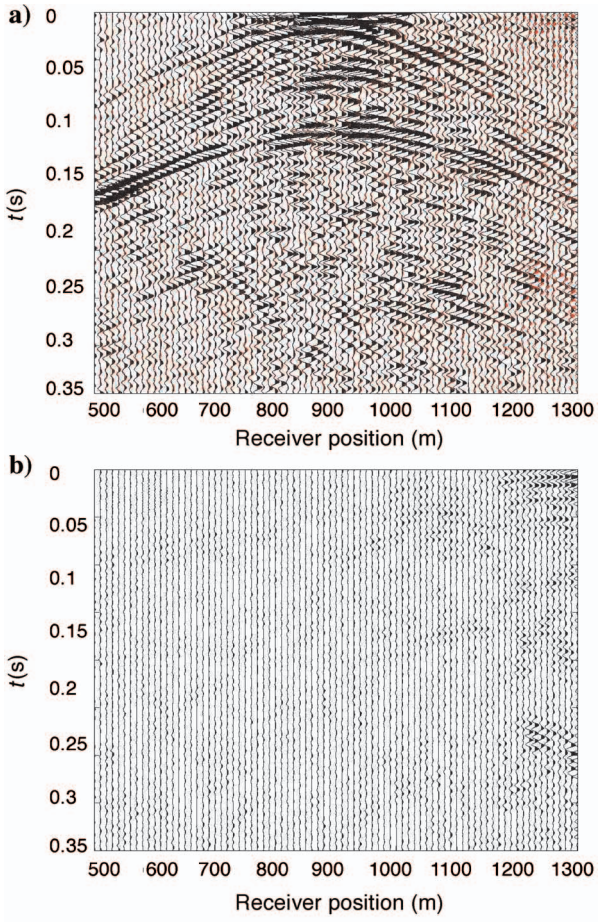

Figure 12. (a) Fixed VS gather (X = 900 m) computed from first (red) and second shifted shot line (black). (b) Difference between two VS gathers above shown with the same amplification.

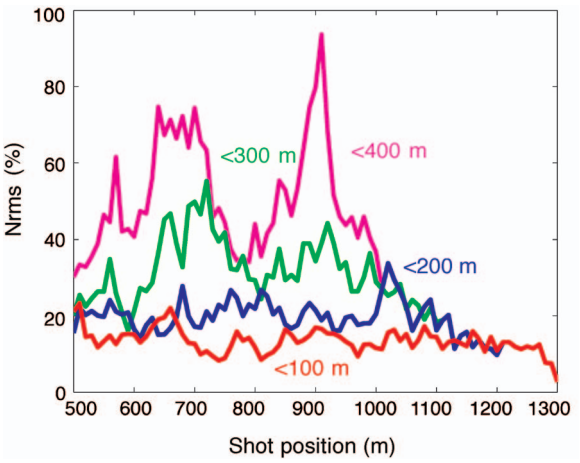

Figure 13. Nrms computed between two VS data sets with shifted shot lines. Shown is Nrms value averaged over the VS gather as a function of VS position. Time window $0 \leq t \leq 370$ ms is used. The number for each plot identifies maximum offset (VS-receiver distance) preserved for each shot gather. Note that full-offset, surface-to-downhole data were used for VS generation.

FIELD CASE STUDY OF 4D VSP

We acquired 4D VSP data as part of a comprehensive monitoring data set at the Peace River field in Canada. A detailed description of the setting and the complete data set can be found in McGillivray (2004). A slanted well was used, containing 50 3C geophones under a surface line of 100 shots (Figure 14). Simultaneously, the same shot line was acquired with both downhole and surface receivers. We concentrate on the baseline data set before a first steam cycle (September, 2002) and a monitor data set (December, 2002) at the end of this steam cycle.

The surface data were processed through a standard processing workflow that included static corrections followed by imaging with a 1D velocity model. If we generate synthetic VSP seismograms based on this estimated 1D model and compare them with field VSP records (Figure 15), we see good agreement in kinematics of the first arrival. In addition to the first arrivals, however, the field data contain many scattered signals from the heterogeneous glacial deposits in the near surface. This scattering is not handled by conventional surface processing and leads to deterioration of useful signal during imaging.

In the downhole data, despite cementing geophones and repeating shots from the same cased shotholes, we were unable to achieve

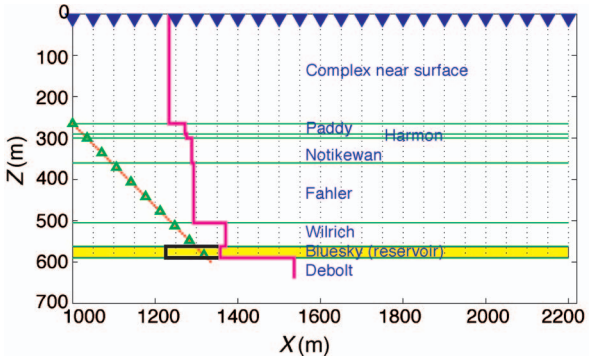

Figure 14. Acquisition geometry of 4D VSP at Peace River, Canada. Receivers (▲) are placed in slanted well and shots (▼) are at the surface. The magenta curve shows the approximate P-wave impedance distribution for the baseline survey, and the black curve shows expected impedance for the monitor survey (after steam injection).

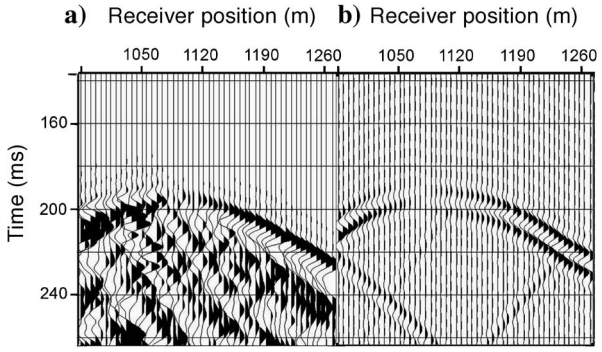

Figure 15. Raw VSP shot gather (a) against full-waveform synthetics (b) based on a seismic 1D velocity model. Note the strong scattering signal after the first arrivals that is not captured by the seismic velocity model.

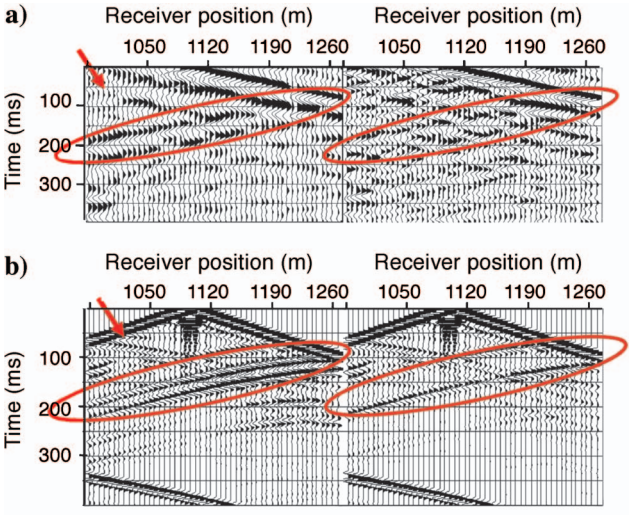

Figure 16. Comparison of prestack VS data (a) with downhole synthetics (b) where sources are fired at the locations of downhole geophones. The reservoir arrivals shown inside red contours are easily identifiable on both records.

good repeatability because the source waveforms and the near surface changed between the surveys. First, the direct P-wave arrivals were delayed on average by 2 ms for December compared with September. Direct S-wave arrivals were delayed by 20 ms. Second, the comparison of rms energy levels of identical traces from the September and December data sets reveals large variations, from 25% to 250%. These differences cannot be removed by a simple scaling factor. Therefore, differences of time-shifted and scaled traces are dominated by near-surface changes rather than by reservoir anomalies. With a straightforward generation of prestack VS data, we were able to reveal events of interest that show good qualitative agreement with downhole synthetics generated with physical sources fired in the place of the VSs (Figure 16). Notice that the upgoing direct wave, marked by a red arrow on Figure 16, is present in the downhole synthetics, but is absent on the VS records because of the downward radiation pattern of the VS, as explained in Appendix C.

PSDM with a 1D velocity model derived from surface seismic generates satisfactory images from the VS data shown on Figure 17. An identical portion of the subsurface imaged with the surface seismic, using exactly the same shots, is shown on Figure 18. As a result of a sufficiently strong 4D change, the VS and surface images give compatible results. First, the amplitude of the top reservoir reflection becomes brighter on the monitor survey. This is caused by an imped-

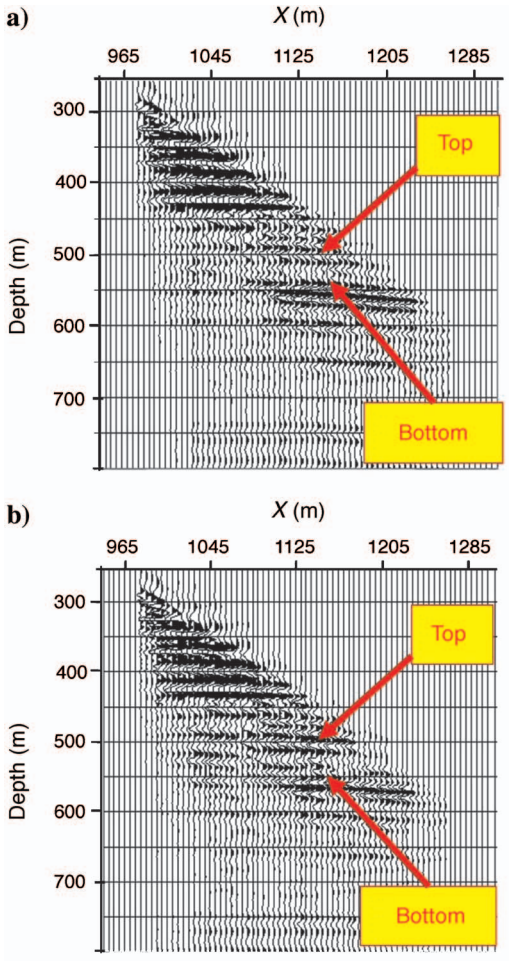

Figure 17. Final images of VS data after PSDM with a portion of the seismic 1D velocity model below the well. Arrows identify top and bottom reservoir on baseline (a) and monitor (b) images.

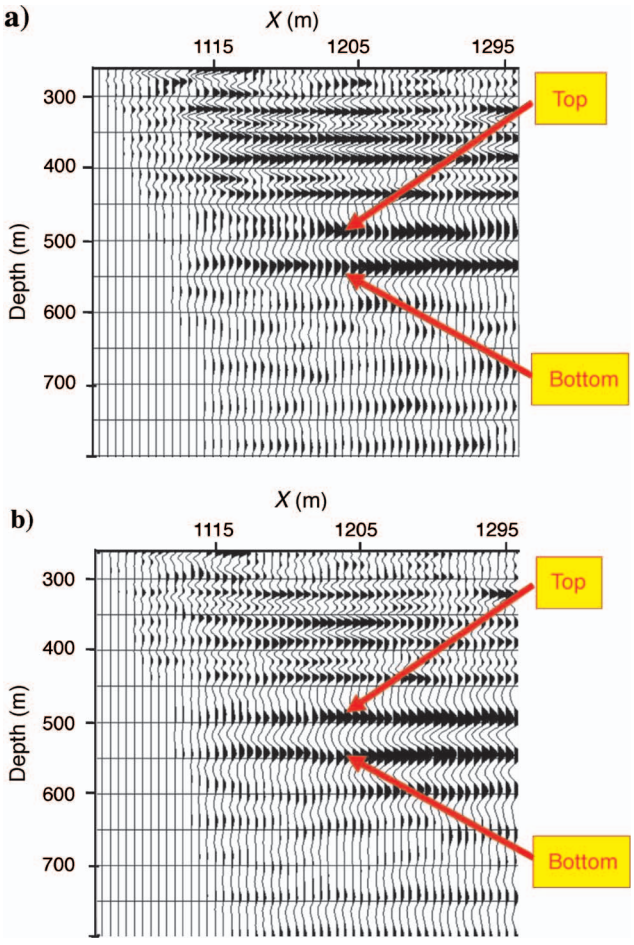

Figure 18. Same subsurface section as on Figure 17, but obtained by surface-seismic data after PSDM with a 1D velocity model. Arrows identify top and bottom reservoir on baseline (a) and monitor (b) images.

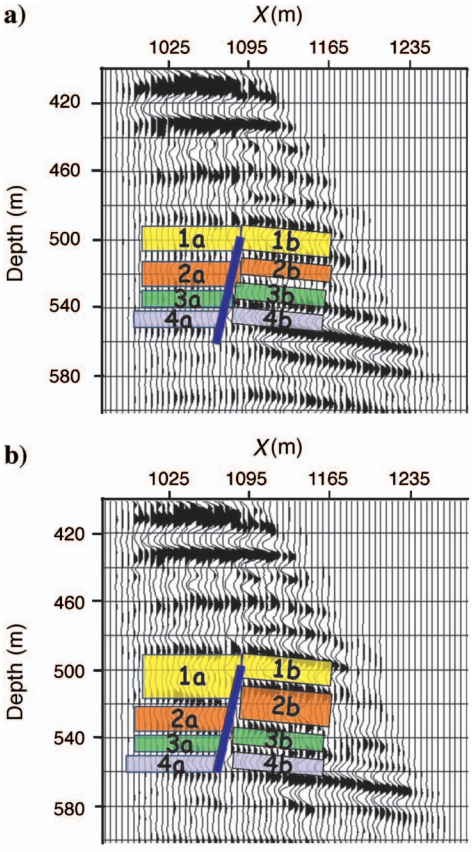

Figure 19. Zoomed reservoir section from Figure 17 for baseline (a) and monitor (b) surveys. VS images allow us to see that intrareservoir compartments expand and contract differently on the left and right sides of the fault in dark blue.

ance decrease in the reservoir resulting from bitumen heating, as suggested by Figure 14. Second, the bottom reservoir interface moves down. This apparent stretch is caused by a combination of velocity decrease and use of the same PSDM velocity model for migration of both 4D data sets, so locally the sections may be considered in pseudotime. In fact, the reservoir also underwent physical dilation, but less than shown.

Details of the images and 4D response, nevertheless, are quite different. The VS images are of much higher frequency and resolution, and contain intrareservoir events (Figure 17) in addition to just top and bottom reservoir as on surface data (Figure 18). Zooming into the reservoir zone, one can start identifying a subtle vertical fault and compartments invisible on surface-seismic images (Figure 19). Small intrareservoir compartments show time-lapse expansion and contraction that occur differently on the right and left side of the fault, thus independently confirming fault location from 4D data. In fact, nearly all of the changes are associated with zones 1a and 2b (Figure 19), showing significant vertical compartmentalization.

To appreciate the quality of the 4D signal from the VS image, look at the repeatability of the time-lapse signal. Overburden events on the surface seismic (Figure 18) show variation in signal strength that is of the same order as the 4D signal from the reservoir. This indicates poor repeatability and casts some doubt on interpretation of reservoir signal. In contrast, the VS data, as expected from synthetic tests, show excellent repeatability (Figure 17). Zooming into the

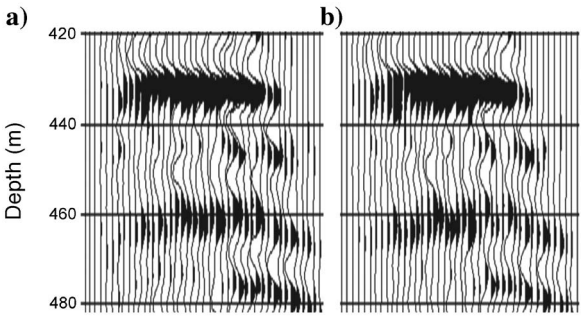

Figure 20. Overburden zoom from VS images for baseline (a) and monitor (b) data illustrating excellent repeatability of the VS data.

section above the reservoir (Figure 20), observe that even individual waveform aberrations repeat almost perfectly, confirming that they are caused by repeatable distortions such as scattering from unchanged heterogeneities and not by nonrepeatable factors.

Overall, the field data example strongly confirms the advantages expected from applying the VSM: We obtained sharp, highly repeatable images despite complex overburden, time-variant near-surface conditions, and different shot wavelets. This was achieved without knowing or needing any velocity model above the receiver borehole or any changes in that model between the surveys. An obvious downside is the reduced extent of coverage illuminated by a VS image compared with conventional VSP data, but now we can have both.

CONCLUSIONS

The VSM relies on the conventional acquisition approach for a VSP, but introduces a new paradigm for how to treat the acquired surface-to-downhole data. It offers the opportunity to eliminate completely the common problem present in conventional imaging approaches — building an accurate velocity model of the near surface. The direct measurement of the transmitted wavefield is combined with time-reversal logic in order to generate a new virtual data set with both sources and receivers downhole. Time reversal is a property of the wave equation in arbitrary heterogeneous and anisotropic media. Therefore, the method is robust and does not rely on ray theory or any other commonly used approximations that break down with realistic heterogeneity that cannot be determined. Reliable VS data may be generated successfully even for strongly heterogeneous (anisotropic) overburden.

We demonstrated that, contrary to most methods, strongly scattering near-surface conditions may even help the quality of VS data by allowing wider offsets in the VS data than for homogeneous overburden. Heterogeneity also allows some relaxation of shot sampling requirements below those required for conventional imaging with homogeneous overburden. The VSM, therefore, is not only able to handle a complex near surface, but indeed extracts benefits from overburden complexity. Being a full elastic wave-equation method, the VS approach has the potential to collapse the energy of the multiple, converted, and diffracted waves into useful primaries. Thus, much of what is typically considered noise in conventional imaging techniques may become part of useful signal in the VSM.

Besides being a useful imaging tool, the VSM offers especially important improvements in 4D seismic monitoring. The ability to relax the requirements of repeating the exact shooting geometry is an advantage that could make 4D monitoring practices more economi-

cal and flexible. Another major advantage is the automatic correction for time-variant, near-surface changes between the surveys. These problems are limiting factors for the repeatability of both marine and land surveys. As shown by the field data example, correction for near-surface changes is inherently included in the VS approach at no extra effort or cost. The VSM also offers the opportunity of generating multicomponent, pure shear-wave data.

ACKNOWLEDGMENTS

We thank Shell Canada for permission to show the VSP data and acknowledge Shell International Exploration and Production for permission to publish this paper. We are extremely grateful to many of our Shell colleagues without whom this study would never have been completed: Charles Jones for processing help and trials; Peter McGillivray for help with the Peace River case study; Paul Milcik for teaching us how to use various imaging tools; and Richard Cook, Barbara Yantis, Boudewijn Salomons, and Uwe Kaestner for invaluable insights into seismic migration.

APPENDIX A

SELECTION OF WINDOW FOR TIME REVERSAL

In our synthetic study, we did not use full traces $S_{k\alpha}(t)$ for time reversal as described by equation 1. Instead, we used only a small time window taken from each trace, centered around the first arrivals. The trace portion used for time reversal and generation of the VS data in our synthetic-data example is depicted on Figure 5 for a receiver at $X = 900$ m. We muted all samples below the hyperbolic yellow line (Figure 4). Exactly the same fixed-hyperbolic mute was applied to every single shot gather along the profile.

Such a mute is compatible with our objective of obtaining good-quality PP reflections while attenuating other wave types, such as PS and SP. One thing we know about the observed wavefield is that in the vicinity of the first arrivals, we do have the strongest dowmgoing PP energy, whereas, at later times, records become contaminated by other wave types. We were unable to separate the wavefield properly because of its complexity, so we decided to mute the later energy. This choice restricts us to the use of primary and short-period reverberation energy only in this example. With up and down wavefield separation, we may use more multiple energy. Trials indicated that using data without muting indeed creates more noisy seismograms, with more obscured PP reflections.

It is somewhat surprising that such a simple approach produces such high-quality results. The mute position does not appear very critical. It should, however, contain all the wavelet we wish to deconvolve. This indicates the robustness of the procedure, but more trials and implementation of deconvolution are required before we develop a best practice. This is rather like the choice of autocorrelation length in deconvolution.

APPENDIX B

EFFECT OF APERTURE ON VS RECORDS

Ray-theory considerations suggested that major contributions to a particular VS trace (equation 1) should come from the vicinity of the specular ray, while the rest will mainly add noise. This data set did

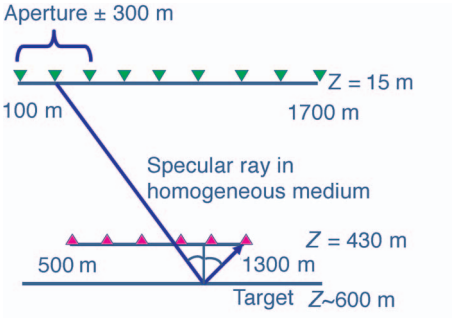

Figure B-1. Simple 1D earth with a constant velocity is used to predict specular ray. A limited aperture of ±300 m is centered around the surface point of emergence of the specular ray.

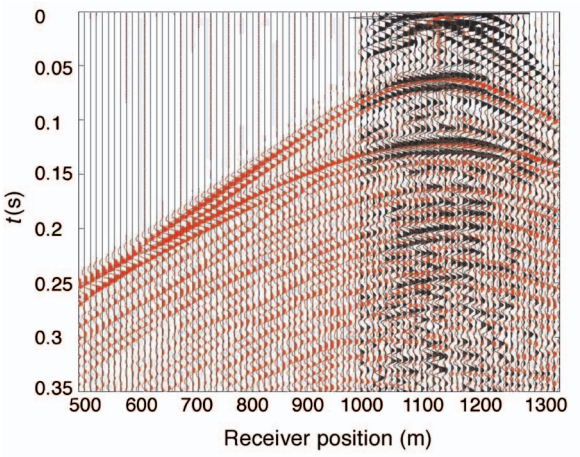

Figure B-2. Same as Figure 8a, but the summation in equation 1 is performed only over the limited aperture depicted in Figure B-1. Note that for the VS gather (black), we can only reconstruct offsets up to 120 m (VS is at $X = 1100$ m).

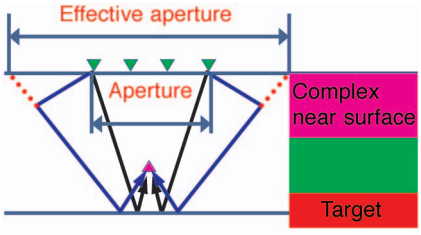

Figure B-3. For any selected receiver (▲) in homogeneous media, the aperture of the source array (▼) is bounded by the ends of black rays emanating from the first and the last sources. For a heterogeneous near surface, the effective aperture is wider because scattering returns to the receiver energy that was originally emitted sideways from the source (sketched by blue arrows).

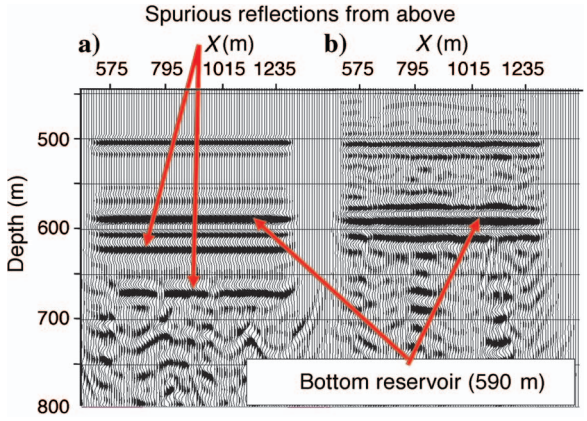

Figure C-1. PSDM images obtained from data acquired with real downhole sources (a) and with VSs (b). Notice the presence of spurious events on image (a) and their absence on the VS image (b). See text for explanation.

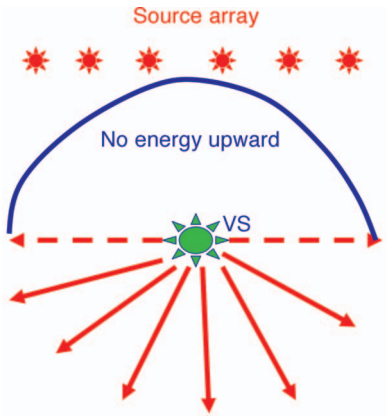

Figure C-2. The VS radiates mainly downward because the surface array originally captured only the upgoing part of the wavefield, while the downgoing part was lost.

not support this expectation. To illustrate, compare the previously shown VS data obtained with full aperture and other data computed with limited aperture, as explained by Figure B-1.

Figure B-2 shows that with a limited aperture, we were only able to reconstruct offsets up to 120 m, whereas with the full aperture, we can obtain VS data with offsets up to 800 m (Figure 8a). The only way to explain this is to assume that energy scatters sideways in the near surface and then propagates back to the deeper subsurface, thus increasing the effective aperture of our surface array (Figure B-3). Such an effect is closely related to so-called superresolution in acoustics (Tsogka and Papanicolaou, 2002; Blomgren et al., 2002) where the same time-reversal mirror (e.g., source array) provides better focusing through random heterogeneous media than through its homogeneous counterpart. This explains our claim that the more complex the overburden, the better for VSs.

APPENDIX C

RADIATION PATTERN OF VSs

The greater control available with VSs gives them characteristics superior to those of real physical sources. When acquiring single-well reflection data along a horizontal wellbore with real physical sources, we expect reflections from both above and below the well. Although we are interested only in reflections from the target zone below, the reflections from above are still present (as artifacts) in our data. These may be imaged if the velocity model is somewhat similar above and below the horizontal well. Indeed, if we perform PSDM of a downhole data set acquired with the real physical sources instead of VSs, we notice the presence of spurious events that represent imaged reflections from above (Figure C-1a). Migration imaged them, because their moveout happened to be close to that predicted by the part of the velocity model below. In the VS image (Figure C-1b), these spurious events are either absent or much weaker.

These results may be explained by the advantageous radiation pattern of the VS. To reproduce the radiation of a downhole physical source in all directions with time reversal, we would have to record the wavefield on a closed surface surrounding the source on Figure 6a (Fink et al., 2000; Fink and Prada, 2001). Because our actual sources are only at the surface above the geophone or VS, in the time-reversal process we are unable to capture energy radiating downward from the VS. The downward part of the wavefield is permanently lost. This implies that in the reverse experiment (Figure 1b), we can collapse energy into our VS only from the upper hemisphere; therefore, the VS will radiate mainly downward (Figure C-2). This feature of a VS is beneficial for imaging targets below the well and creates a superior image with fewer artifacts than would be a case from a real downhole source emitting energy in all directions.

Another advantage is that we actually know the outgoing wavelet and can make it perfectly zero-phase with scattered and short-period reverberation, all at time zero.

REFERENCES

Blomgren, P., G. Papanicolaou, and H. Zhao, 2002, Superresolution in time-reversal acoustics: Journal of the Acoustical Society of America, **111**, 230–248.

Chakroun, N., M. Fink, and F. Wu, 1995, Time reversal processing in ultrasonic nondestructive testing: IEEE Transactions on Ultrasonics, Ferroelectrics and Frequency Control, **42**, 1087–1098.

de Rosny J., and M. Fink, 2002, Overcoming the diffraction limit in wave physics using a time-reversal mirror and a novel acoustic sink: Physical Review Letters, **89**, 124301.

Draeger, C., D. Cassereau, and M. Fink, 1998, Acoustic time reversal with mode conversion at a solid-fluid interface: Applied Physics Letters, **72**, 1567–1569.

Fink, M., D. Cassereau, A. Derode, C. Prada, P. Roux, M. Tanter, J.-L. Thomas, and F. Wu, 2000, Time-reversed acoustics: Reports on Progress in Physics, **63**, 1933–1995.

Fink, M., and C. Prada, 2001, Acoustic time-reversal mirrors: Inverse Problems, **17**, R1–R38.

Hardage, B., 2000, Vertical seismic profiling: Principles: Elsevier Science Publications Co., Inc.

McGillivray, P. R., 2004, Microseismic and time-lapse monitoring of heavy oil extraction process at Peace River: 74th Annual International Meeting, SEG, Expanded Abstracts, 572–575.

Tsogka, C., and G. Papanicolaou, 2002, Time reversal through a solid-liquid interface and super-resolution: Inverse Problems, **18**, 1639–1657.